ELSEVIER

Physica C 382 (2002) 251–262

PHYSICA C

www.elsevier.com/locate/physc

Strengthened, biaxially textured Ni substrate with small alloying additions for coated conductor applications

A. Goyal *, R. Feenstra, M. Paranthaman, J.R. Thompson, B.Y. Kang, C. Cantoni, D.F. Lee, F.A. List, P.M. Martin, E. Lara-Curzio, C. Stevens, D.M. Kroeger, M. Kowalewski, E.D. Specht, T. Aytug, S. Sathyamurthy, R.K. Williams, R.E. Ericson [1]

Oak Ridge National Laboratory, Metals and Ceramics Division, P.O. Box 2008, Oak Ridge, TN 37831-6116, USA

Received 14 August 2001; accepted 18 December 2001

Abstract

Fabrication of a biaxially textured, strengthened Ni substrate with small alloying additions of W and Fe is reported. The substrates have significantly improved mechanical properties compared to 99.99% Ni and surface characteristics which are similar to that of 99.99% Ni substrates. High quality oxide buffer layers can be deposited on these substrates without the need for any additional surface modification steps. Grain boundary misorientation distributions obtained from the substrate show a predominant fraction of low-angle grain boundaries. A high critical current density, J_c, of 1.9 MA/cm^2 at 77 K, self-field is demonstrated on this substrate using a multilayer configuration of YBCO/CeO_2/YSZ/ Y_2O_3/ Ni–3at.%W–1.7at.%Fe. This translates to a I_c/width of 59 A/cm at 77 K and self-field. J_c at 0.5 T is reduced by only 21% indicating strongly-linked grain boundaries in the YBCO film on this substrate.
© 2002 Elsevier Science B.V. All rights reserved.

1. Introduction

Fabrication of high temperature superconducting (HTS) wires based on epitaxial deposition of superconductors on biaxially textured substrates currently forms a central, world-wide research thrust [1–4]. Conductors can be fabricated by epitaxial deposition of YBCO and other superconducting materials on biaxially textured substrates produced by three techniques—ion-beam assisted deposition (IBAD [1]), inclined substrate deposition (1SD [2]) and rolling-assisted biaxially textured substrates (RABiTS [3,4]). In the RABiTS technique, biaxial texture is first produced in a metal substrate followed by epitaxial deposition of oxide buffer layers and the superconductor. This technique employs simple, well-established, and industrially scalable thermomechanical processing to obtain biaxial textures as good as 6° full-width-half-maximum (FWHM) [5]. Critical current densities approaching 3 MA/cm^2 have been reported for epitaxial YBCO films on substrates fabricated using the RABiTS technique [6].

* Corresponding author. Tel.: +1-423-574-1587; fax: +1-423-574-7659.

E-mail address: goyala@ornl.gov (A. Goyal).

[1] 3M Company, Corporate Analytical Technical Center, P.O. Box 33221, MS 201-2S-16, St. Paul, MN 55144-3321, USA.

0921-4534/02/$ - see front matter © 2002 Elsevier Science B.V. All rights reserved.
PII: S0921-4534(02)00626-3

Much of the work reported so far, which demonstrates high J_c conductors (i.e., $J_c > 1$ MA/cm^2) using the RABiTS technique, employs a high purity Ni (99.99%) metal template. The reported substrate thickness ranges from 50 to 125 μm, with the desired thickness of the substrate being 50 μm for maximization of the engineering critical current density (J_c). However, high purity Ni strips that are only 50 μm thick are mechanically very weak and can bend easily. Hence, handling of these textured Ni strips is non-trivial and may introduce significant defects (bends, kinks, etc.) in a long length manufacturing process. It would be desirable to work with alloy substrates which are much stronger and also have the required high degree of texture. Alloy substrates are also required in applications where AC losses from the Ni substrate are a significant issue. Fabrication of biaxially textured alloy substrates which are both strong and non-magnetic has been reported [7]. However, since the surface characteristics of Ni-alloy substrates with high alloying additions (which are required to make Ni non-magnetic) is significantly different from that of pure Ni substrates, additional surface modification steps are required in order to deposit high quality epitaxial oxide layers [8]. Therefore, it is of interest to fabricate a substrate which has significantly improved mechanical properties compared to Ni but with surface characteristics similar to those of pure Ni substrates, so that no additional surface modification steps are required. Such substrates could find use in applications where AC losses are not a significant issue.

In this paper, we report on the fabrication of biaxially textured, strengthened Ni substrates with small alloying additions of W and Fe. The substrates have significantly improved mechanical properties compared to 99.99% Ni and surface characteristics which are similar to those of the pure Ni substrates. High quality oxide buffer layers can be deposited on these substrates without the need for any surface modification. Grain boundary misorientation distributions (GBMD) obtained from the substrates suggests the predominant fraction of grain boundaries is low-angle. A range of oxide buffer layers can be directly deposited with an epitaxial, cube-on-cube orientation on these substrates. Lastly, we demonstrate that high J_c and high-I_c films can be fabricated on such substrates.

2. Experimental

Alloys of composition Ni–3at.%W–2at.%Fe were fabricated using powder metallurgy. The composition of the alloy was determined using a Perkin Elmer Optima 3300 DV inductively coupled plasma (ICP) analysis to quantify for 29 elements. After compaction and coil formation, the alloy strips were rolled in a reel-to-reel tension rolling mill to total deformations greater than 98%. The reduction per pass at each stage was ~10%. After the final rolling, the substrates were annealed at various temperatures (1000–1400 °C) for 1 h in flowing Ar/4%H_2 or in a vacuum furnace with an effective oxygen partial pressure, $p(O_2)$, $<10^{-8}$ Torr.

Mechanical properties were measured on fully-annealed, cube-textured, laser machined, tensile-test specimens, conforming to a dog-bone geometry with a gauge section 5 mm wide and 25 mm-long. Tensile tests were performed using a standard electromechanical testing machine (Mod. Instron 4500) at a constant cross-head displacement rate of 1.5 mm/min with the stress applied along the [1 0 0] crystallographic axis of the biaxially textured substrate (i.e. the *a*-axis was along the tensile axis). The specimens were gripped using a pair of mechanical wedge-type grips and the deformation of the specimen in the gauge section was recorded using a clip-on extensometer (see inset Fig. 3). Magnetic properties of the alloy substrate were characterized using a superconducting quantum interferenced device (SQUID) magnetometer from room temperature down to 5 K.

CeO_2 seed layers were deposited directly on biaxially textured Ni–3at.%W–2at.%Fe substrates using reactive electron beam evaporation at a substrate temperature of 600 °C. The deposition rate was chosen to be 1 Å/s and the water partial pressure was controlled at 3×10^{-6} Torr and the film thickness was 100 Å. Y_2O_3 seed layers were also deposited directly on biaxially textured Ni–W

substrates using reactive e-beam evaporation. Conditions for deposition of Y_2O_3 on Ni have been described previously [9] and are also summarized here. The Y_2O_3 seed layers were grown on the Ni–W substrates at 650 °C. The background H_2O pressure was maintained around 1×10^{-5} Torr. The H_2O pressure supplied in the chamber is sufficient to oxidize the film to the stoichiometric Y_2O_3. The deposition rate was 2 Å/s, and the final thickness was around 500 Å. The measured partial pressure, pO_2 was in the range of 10^{-8} Torr during deposition.

For deposition of solution seed of Gd_2O_3 layer, a 2-methoxyethoxide solution of gadolinium methoxyethoxide was dip-coated onto the Ni–3at.%W–2at.%Fe substrate using a procedure described elsewhere for coating of Ni [10]. The films were subsequently annealed at 1160 °C for 1 h in flowing 4% H_2 and 96% Ar.

Subsequent to the deposition of seed oxide buffer layers by e-beam evaporation, Rf-magnetron sputtering technique was used to deposit additional layers of YSZ and CeO_2 to complete the buffer layer stack for subsequent deposition of YBCO [11,12]. Ni–3at.%W–2at.%Fe substrates with the epitaxial seed oxide layer were mounted onto the substrate heater and the system was evacuated to a pressure of 1×10^{-6} Torr. The chamber was then back-filled with Ar/H_2 (4%) gas to 5×10^{-2} Torr and the substrate was then heated to 780 °C. After holding for 15 min, the pressure was reduced to 1×10^{-2} Torr and sputtering commenced using an on-axis target. The thickness of the YSZ layer deposited was ~0.4 μm. Subsequent to the deposition of YSZ, a thin (~200 Å) and dense CeO_2 layer was deposited by Rf sputtering to complete the buffer layer structure.

The CeO_2-buffered YSZ/Y_2O_3/Ni–3at.%W–2at.%Fe substrates were annealed under N_2 at 650 °C for 0.5 h prior to the YBCO precursor deposition. Ex-situ YBCO precursors were deposited on CeO_2-buffered YSZ/Y_2O_3/Ni–3at.%W–2at.%Fe substrates using electron beam co-evaporation of Y, BaF_2, and Cu using the experimental conditions reported earlier [13,14]. The YBCO precursor films were shiny, brown-black in color, and stable in air. The YBCO film thickness was 3000–3200 Å. The YBCO precursor films were heated to 100 °C in flowing Ar or N_2 gas and then H_2O with a dew point of 40–60 °C and a pO_2 of 180–260 ppm were introduced into a tubular furnace with linear gas flow conditions. The H_2O dew point of 40 °C corresponds to approximately 55 Torr of pH_2O. The low pO_2 gas atmosphere was prepared by mixing high purity Ar gas with Ar/O_2 (2%) gas mixtures. The gas flow used was 0.5–2 l/min. The furnace was ramped to 730 °C in 15 min followed by a slow ramp to 740 °C in another 5 min. The furnace was kept at 740 °C for 80 min. During the annealing process, wet gas was switched to dry gas after 50 min of reaction. The sample was then cooled to 500 °C in 20 min and switched from low pO_2 to pure 1 atm O_2. The film was kept at 500 °C for 30 min in O_2 before furnace cooling to room temperature. The high temperature anneal under wet conditions resulted in the conversion of the Y, BaF_2, and Cu into $YBa_2Cu_3O_{7-y}$.

A Philips model XRG3100 diffractometer with Cu K_α radiation was used to record powder diffraction patterns. A Picker four-circle diffractometer was used to determine the texture of the films by ω- and ϕ-scans. Pole figures were collected for all the layers to determine the percentage of cube texture. The thicknesses of both buffers and YBCO films were determined by Rutherford backscatter spectroscopy (RBS). The resistivity and transport critical current density, J_c, were measured using a standard four-probe technique. The voltage contact spacing was 0.4 cm. Values of J_c were calculated using a 1 μV/cm criterion.

3. Results and discussion

3.1. Biaxially textured metal substrate

Chemical analysis of substrate material by ICP indicated the composition of the substrate to be Ni–3at.%W–1.7at.%Fe. Fully rolled samples 50 μm thick were annealed under different conditions of temperature and time. Fig. 1 shows linear and logarithmic scale (1 1 1) pole figures for Ni–3at.%W–1.7at.%Fe samples that were annealed between 1100 and 1400 °C for 1 h in flowing Ar–4%H_2. For lower annealing temperatures, significant amounts of retained texture is present. Even

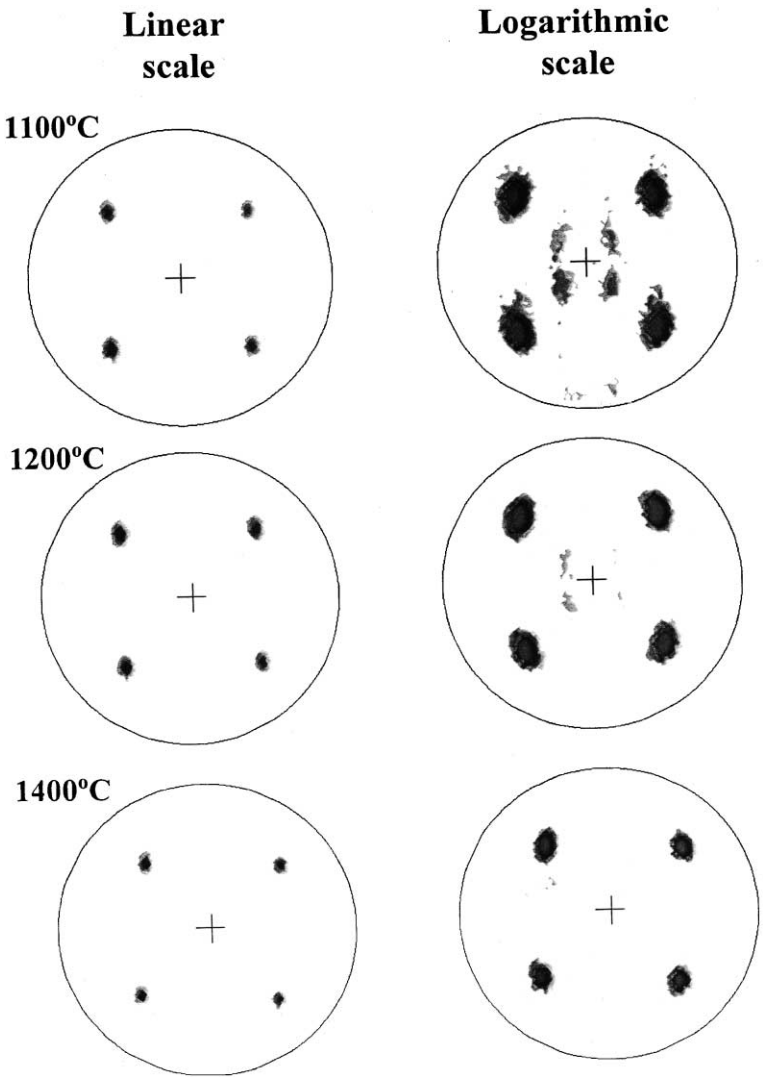

Fig. 1. (1 1 1) X-ray pole figures for Ni–3at.%W–1.7at.%Fe alloy substrate plotted in linear and logarithmic scales for annealing at various conditions: (a) 1100 °C for 1 h in 4%H_2/Ar; (b) 1200 °C for 1 h in 4%H_2/Ar; (c) 1400 °C for 1 h in 4%H_2/Ar.

after annealing at 1100 °C the substrate is only 98% cube textured. Small components (1–2%) of untextured material can result in a significant fraction of undesirable high-angle grain boundaries as has been determined using electron backscatter Kikuchi diffraction [8]. For the sample annealed at 1200 °C for 1 h in flowing Ar–4%H_2, ~100% cube texture is present. Only the peaks corresponding to the $\{1\,0\,0\}\langle 1\,0\,0\rangle$ cube orientations can be seen in both the pole figures indicating a fully textured material. Quantitative analysis of the pole figure intensities shows that the substrate is essentially 100% cube textured. Table 1 summarizes the texture obtained for annealing at different temperatures for 1 h in flowing Ar–4%H_2. On annealing at 1200 °C, the in-plane texture as determined by a (1 1 1) ϕ-scan was found to be 7° FWHM. The FWHM for the out-of-plane texture as determined by an ω-scan was found to be 6.1° and 8.8° for rocking in and about the rolling

Table 1
Details of annealing conditions and resulting cube texture

	Ni–3at.%W–1.7at.%Fe	Heat treatment
% Cube	98.5%	1100 °C, 60 min, slow rates
ϕ		
ω ($\phi = 0$)		
ω ($\phi = 90$)		
% Cube	99.6%	1200 °C, 60 min, slow rates
ϕ	7.0°	
ω ($\phi = 0$)	6.1°	
ω ($\phi = 90$)	8.8°	
% Cube	99.8%	1300 °C, 60 min, slow rates
ϕ	6.8°	
ω ($\phi = 0$)	5.2°	
ω ($\phi = 90$)	8.9°	
% Cube	100%	1400 °C, 60 min, slow rates
ϕ	5.8°	
ω ($\phi = 0$)	4.3°	
ω ($\phi = 90$)	7.4°	

direction. Upon annealing at 1400 °C, the texture sharpened considerably with the FWHM of the in-plane texture decreasing to 5.8°. The out-of-plane texture also sharpened to FWHM of 4.3° and 7.4° respectively.

Fig. 2a shows an orientation image of the substrate annealed at 1200 °C and created solely from crystallographic data obtained using electron backscatter Kikuchi patterns (EBKP) obtained in a scanning electron microscope. The technique of EBKP as applied to such substrates is described in detail elsewhere [15]. Briefly, in order to generate an orientation image micrograph (OIM), data are gathered in a hexagonal grid of spacing typically a fraction of the average grain size in the sample. At each point of the hypothetical hexagonal lattice, an EBKP pattern is captured, indexed and its orientation stored in a file. At the end of the scan the output file contains information regarding the location and orientation of each point in the scan. Micrographs are constructed by placing a hypothetical hexagonal lattice of the hexagonal grid. Grain boundary misorientations are then calculated for all resulting grain boundaries. The OIM

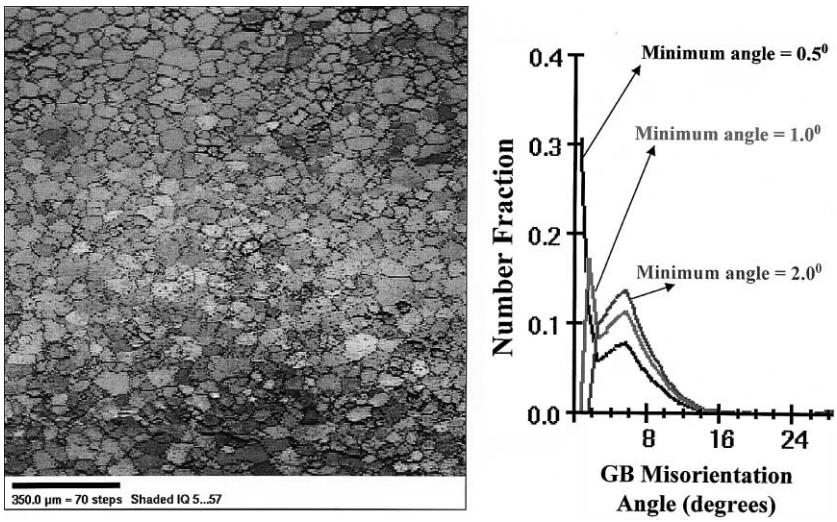

Fig. 2. (a) OIM from a macroscopic region (>1 mm × 1 mm) of the cube textured Ni–3at.%W–1.7at.%Fe alloy substrate. EBKP were obtained in a hexagonal grid with a step size of 5 μm. Gray level shading on the micrograph is a reflection of the pattern quality or intensity of the Kikuchi bands observed at each point. Indexing of the pattern at each location gave a unique measure of the orientation at that point. A hypothetical hexagonal lattice with a grain size of 5 μm was superimposed at each point from which a pattern was obtained. Resulting grain boundary misorientations were then calculated between each point of the hexagonal lattice and the recreated OIM then showed the position of all grain boundaries in the area examined, (b) GBMD plotted as number fraction of grain boundaries below a certain angle from the region in (a), drawn with different minimum misorientations as the starting point (see text for further details).

micrograph shows the location of all grain boundaries in the sample. It can be seen that the average grain size is ~50 μm. Fig. 2b shows grain boundary misorientation distributions (GBMD) calculated using the data gathered from the region shown in Fig. 2a. Three curves are indicated in the figure and each having a different minimum misorientation angle used to plot the GBMD. The minimum misorientation angles used were 0.5°, 1° and 2° respectively. While for angles less than 2°, it is possible that the GBMD is skewed to lower angles because of a high number of data points coming from *within* a single grain in the substrate, all misorientations greater than 2° can be assumed to define a distinct grain boundary. Examination of the GBMD with a minimum misorientation angle of 2°, indicates a peak at ~5.5°, with a FWHM of ~6°. Such a substrate with predominantly low-angle grain boundaries can be expected to result in high-J_c YBCO films.

Fig. 3 shows results of a tensile test performed on a dog-bone sample Ni–W–Fe sample with the stress applied along the crystallographic *a*-axis of the sample. The graph in the inset shows the region of the curve near yielding at higher magnification. Yield strength (YS) determinations at 0.02% and 0.2% strain are indicated by straight lines intercepting the flow curve. Average of several tests on similar samples gave a YS of 143 and 154 MPa at 0.02% and 0.2% strain respectively. Similar tests for 99.99% Ni (metals basis) show a YS of 40 and 58 MPa at 0.02% and 0.2% strain respectively with the Ni substrates also made using powder metallurgy and having a similar grain size, thickness and annealing condition. Hence, the Ni substrate with minor alloying additions of W and Fe is significantly stronger than the 99.99% Ni substrate. The mechanism by which this improvement in mechanical properties occurs, is believed to be solid solution strengthening.

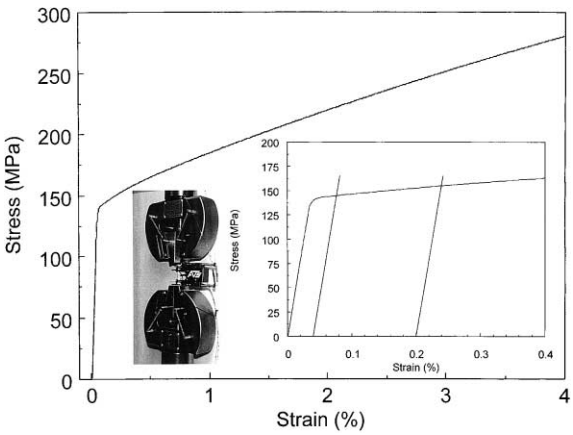

Fig. 3. Tensile test data obtained on a laser machined, dog-bone tensile specimen of an annealed Ni–3at.%W–1.7at.%Fe alloy substrate. The sample was cut in a manner such that the long axis of the sample is parallel to the crystallographic *a*-axis or parallel to the [1 0 0] direction. The insets show the mechanical wedge-type grips and the clip on extensometer used for the test as well as the region of the tensile curve near yielding at higher magnification.

The magnetic properties of the Ni–3at.%W–1.7at.%Fe substrate were examined at cryogenic temperatures. A slab of dimensions $5 \times 5.5 \times 2$ mm^3 (0.4756 g) was loaded into a SQUID-based magnetometer. The magnetic field was applied parallel to the long edge of the sample to minimize demagnetization effects, since the alloy is ferromagnetic at all temperatures studied ($T < 300$ K). To assess the temperature dependence of the mass-based magnetization $M = (\text{magnetic moment})/(\text{sample mass})$, a magnetic field of 1 kOe was applied that magnetized the slab to within ~10% of saturation. Then the temperature T was swept from 5 to 300 K and back to 5 K. The results are shown in Fig. 4, where it is evident that M varies very little for temperatures below ~150 K. The inset shows the field dependence of M at 100 K, for fields up to 65 kOe, revealing a "square" response characteristic of a soft ferromagnet. As expected, the saturation magnetization of 40 G cm^3/g lies significantly below that of pure Ni (57.5 G cm^3/g at $T = 0$). Compared with the (interpolated) previously reported value of 37.7 for Ni–3at.%W [16], the present value is slightly higher, which is likely due to the Fe-content of 1.7at.% in the powder metallurgy-processed material. For the binary Ni–W alloy, one expects a value $T_c \approx 450$ K for the Curie temperature [17]. The data in Fig. 4 clearly shows that the Ni–3at.%W–1.7at.%Fe substrate is magnetic and may not be useful in applications that are strongly sensitive to AC losses. However, by increasing the W content, non-magnetic alloys can be fabricated. We have fabricated Ni–9at.%W alloys by vacuum arc melting and optimization of

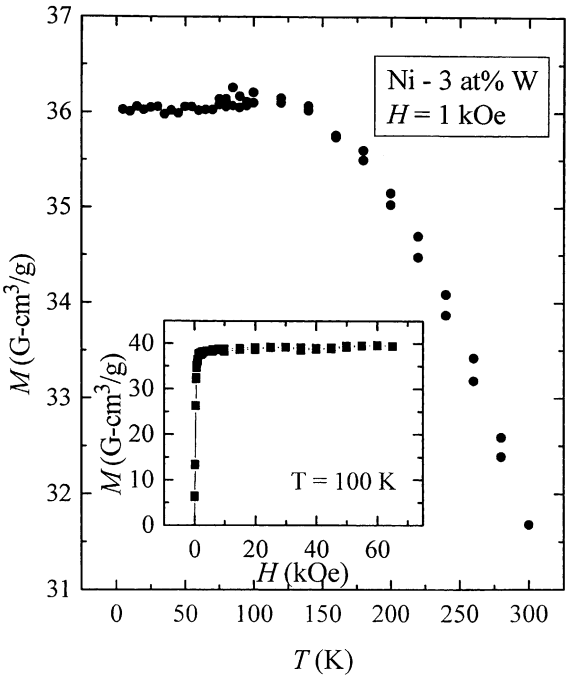

Fig. 4. Magnetization, M, versus temperature for the Ni–3at.%W–1.7at.%Fe alloy substrate measured at $H = 1$ kOe. The inset shows the field dependence of M at 100 K, for fields up to 65 kOe. Refer to text for details.

the thermomechanical processing to obtain ~100% cube textured substrates is in progress.

3.2. Epitaxial seed oxide buffer layer on metal substrate

Let us now consider the epitaxy and properties of the seed oxide buffer layer. Fig. 5a–c shows θ–2θ-scan of CeO_2, Y_2O_3, Gd_2O_3 buffer layers deposited directly on Ni–3at.%W–1.7at.%Fe substrates. 3 mm wide and 25 mm long, and annealed at 1200 °C. CeO_2 and Y_2O_3 were deposited using e-beam evaporation using conditions described in the experimental section. Both figures show the presence of only (2 0 0) oxide peaks. In-plane and out-of-plane textures for both seed layers was similar to that of the alloy substrate.

Fig. 5c shows a θ–2θ-scan of a Gd_2O_3 buffer layer deposited on this substrate under conditions similar to deposition on 99.99% Ni. Again, only the (2 0 0) peak of the oxide is evident. In-plane

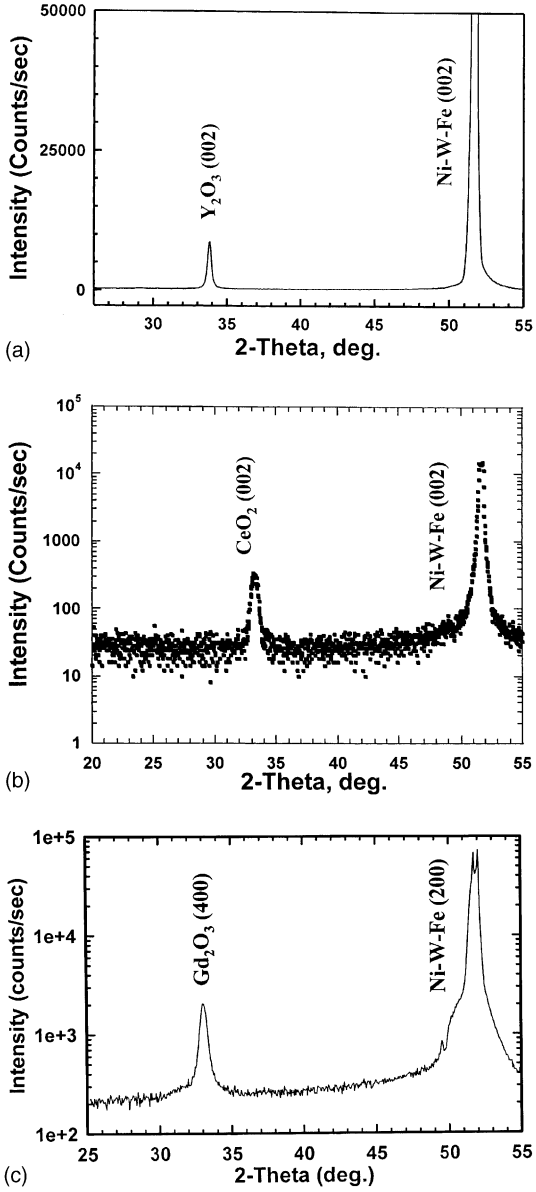

Fig. 5. (a) θ–2θ X-ray data for a CeO_2 layer deposited by electron beam evaporation on a Ni–3at.%W–1.7at.%Fe alloy substrate indicating the presence of only the (2 0 0) peaks of CeO_2 and Ni–3at.%W–1.7at.%Fe alloy substrate; (b) θ–2θ X-ray data for a Y_2O_3 layer deposited by electron beam evaporation on a Ni–3at.%W–1.7at.%Fe alloy substrate indicating the presence of only the (2 0 0) peaks of Y_2O_3 and Ni–3at.%W–1.7at.%Fe alloy substrate; (c) θ–2θ X-ray data for a Gd_2O_3 layer using sol–gel techniques on a Ni–3at.%W–1.7at.%Fe alloy substrate indicating the presence of only the (2 0 0) peaks of Gd_2O_3 and Ni–3at.%W–1.7at.%Fe alloy substrate.

and out-of-plane textures for both seed layers was similar to that of the alloy substrate. The data in Fig. 5 shows that excellent epitaxy can be obtained for various seed layers on the Ni–3at.%W–1.7at.%Fe substrate using the same deposition conditions as used for 99.99%Ni.

It is of interest to determine why no additional surface modification is required for deposition of seed oxide layers on the Ni–3at.%W–1.7at.%Fe substrate. Recent work by Cantoni et al. [18] sheds light on the importance of surface superstructures in controlling the epitaxy of the seed oxide layer on 99.99% Ni. Using reflection high-energy electron diffraction (RHEED) and Auger electron spectroscopy (AES) studies, Cantoni et al. showed that a c(2 × 2) 2-D superstructure due to surface segregation of sulfur is present on the surface of the {1 0 0}⟨1 0 0⟩ Ni substrate, and cannot be removed by typical reducing heat treatments. It was further shown that this superstructure can have a dramatic effect on the heteroepitaxial growth of oxide seed layers. In order to examine and compare the surface superstructure present in the Ni–3at.%W–1.7at.%Fe substrate with that on the 99.99% Ni substrate, RHEED patterns were obtained from the surface of both substrates. Fig. 6a shows a RHEED pattern obtained from the 99.99% Ni substrate with the incident electron beam along the ⟨1 0 0⟩ crystal direction. The substrate temperature was 500 °C. the background pressure was 1.0×10^{-8} Torr and the oxygen partial pressure was 2.0×10^{-10} Torr. Although the diffraction pattern is broadened due to the orientation distribution of the grains (the electron beam samples a few hundreds grains), the RHEED streaks are well-defined and distinct. Scanning the beam over the sample's surface did not change their position. The pattern in Fig. 6a shows two extra streaks (indicated by arrows) in addition to the reflections observed for a clean Ni(0 0 1) surface pattern. The extra streaks are positioned halfway between the Ni streaks and are not observed when the incident beam is parallel to the ⟨1 1 0⟩ direction. This situation is consistent with the presence of a c(2 × 2) superstructure on the {1 0 0}⟨1 0 0⟩ Ni surface [18]. The RHEED pattern in Fig. 6b was acquired under the same conditions used for Fig. 6a, and shows that a very similar surface superstructure is also present on the Ni–3at.%W–1.7at.%Fe substrate. It is speculated that the presence of this superstructure on the Ni–3at.%W–1.7at.%Fe substrate, and the absence of Fe and/or W oxides on the substrate surface permits cube-on-cube epitaxial deposition of oxides without the need for any additional surface modification steps.

3.3. Deposition of additional oxide buffer layers and YBCO

Having formed an epitaxial layer of Y_2O_3 on the biaxially textured Ni-alloy, we then deposited YSZ (400 nm) and CeO_2 (20 nm) oxide layers by

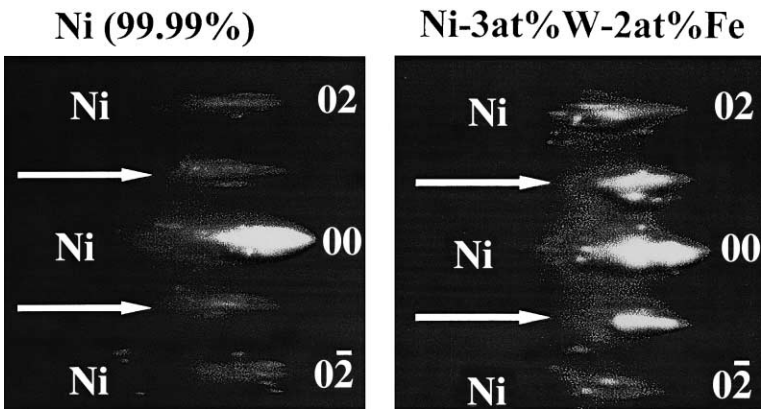

Fig. 6. RHEED patterns obtained with the incident electron beam along ⟨1 0 0⟩ for: (a) 99.99% Ni; and (b) Ni–3at.%W–1.7at.%Fe alloy substrate. The arrows indicate the existence of a c(2 × 2) superstructure in both substrates.

Rf-sputtering using conditions detailed in the experimental section. This was followed by deposition of a YBCO precursor film by co-evaporation of Y, Cu and BaF_2. Deposition conditions for each layer have been summarized in the experimental section. The precursor film was then converted to YBCO using conditions mentioned in the experimental section. Fig. 7a shows ϕ-scan of the various layers in the multilayer sample. The FWHM of the ϕ-scan were 7.3°, 8.1°, 8.3° and 9.1° for the Ni, Y_2O_3, YSZ and YBCO layers, respectively. Since the CeO_2 cap buffer layer was only 20 nm thick and some $BaCeO_3$ forms at the bottom of the YBCO layer, the intensities from this layer are rather weak after conversion to YBCO and hence data from this layer is not shown in Fig. 7. The out-of-plane texture of the various layers for rocking about the rolling direction is shown in Fig. 7b. The FWHM of the ω-scans were 6.2°, 7.4°, 8.5° and 8.6° for the Ni, Y_2O_3, YSZ and YBCO layers respectively. The out-of-plane texture of the various layers for rocking in the rolling direction is shown in Fig. 7c. The FWHM of the ω-scans were 4.6°, 5.4°, 5.4° and 5.7° for the Ni, Y_2O_3, YSZ and YBCO layers respectively. Clearly good epitaxy is obtained through the multilayer stack. The increase in the out-of-plane texture in going from the metal substrate to the oxide layer for these two substrates is assumed to arise because of some visible rolling marks contributing to an increased surface roughness of the metal substrate.

Critical current density was measured at 77 K in self-field for two nominally identical samples made side-by-side during all processing steps. The J_c was measured to be 1.9 MA/cm^2 and 1.6 MA/cm^2 respectively using an electric field criterion of 1 μV/cm. Fig. 8 shows an I–V curve measured at 77 K, self-field for the sample with a J_c of 1.9 MA/cm^2.

Another sample with a width of 1 cm was fabricated using a similar stack of oxide buffer layers with the configuration YBCO/CeO_2/YSZ/Y_2O_3/Ni–3at.%W–1.7at.%Fe. The YBCO layer (3200 Å) was again made using the ex-situ BaF_2 process. The ω- and ϕ-scans for this sample are shown in Fig. 9. The ω-scan shown correspond to rocking the sample *in* the rolling direction. In this case, no increase in the out-of-plane texture in the oxide layer is observed. Transport J_c (77 K, self-field) for this sample was again measured to be 1.9 MA/cm^2. The corresponding I_c was 59.10 A. Fig. 10 shows J_c versus applied magnetic field for this sample. J_c at 0.5 T reduced to only 21% indicating strongly-linked grain boundaries in the YBCO film as expected.

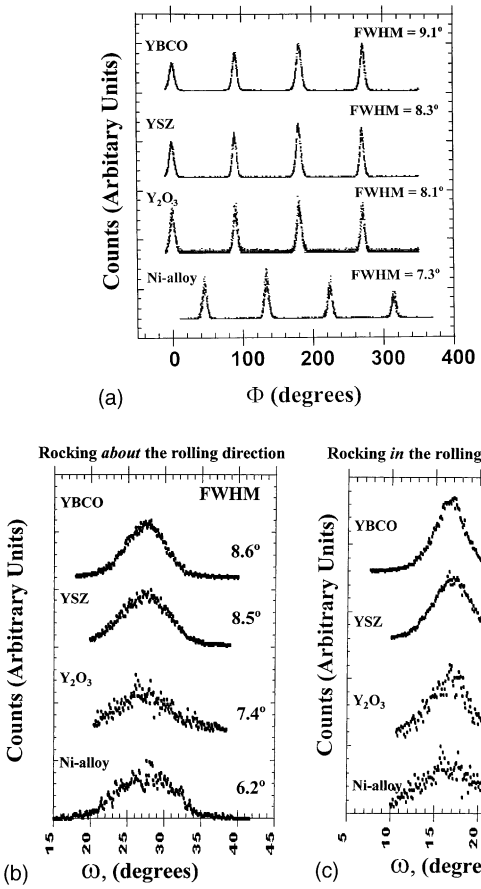

Fig. 7. (a) In-plane texture for the various layers in the multilayer stack of YBCO/CeO_2/YSZ/Y_2O_3/Ni–3at.%W–1.7at.%Fe. X-ray ϕ-scans for the various layers show a good transference of the biaxial texture from the alloy substrate to the YBCO film. The FWHM for the Ni, Y_2O_3, YSZ and YBCO layers was 7.3°, 8.1°, 8.3° and 9.1° respectively. (b) Out-of-plane texture for the various layers in the multilayer stack when the sample is rocked *about* the rolling direction. X-ray Θ-scans show that the FWHM for the Ni, Y_2O_3, YSZ and YBCO layers was 6.2°, 7.4°, 8.5° and 8.6° respectively. (c) Out-of-plane texture for the various layers in the multilayer stack when the sample is rocked *in* the rolling direction. X-ray Θ-scans show that the FWHM for the Ni, Y_2O_3, YSZ and YBCO layers was 4.6°, 5.4°, 5.4° and 5.7° respectively.

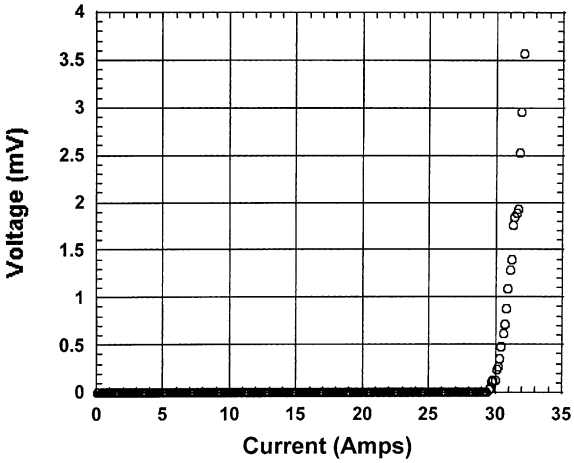

Fig. 8. *I–V* curve for the 1.9 MA/cm^2 sample taken at 77 K, self-field.

4. Summary

Biaxially textured Ni–3at.%W–1.7at.%Fe substrates were fabricated starting with powder metallurgy produced specimens. 100% cube texture was obtained for samples annealed at 1200 °C for 1 h in flowing Ar–4%H_2. The in-plane texture as determined by a (1 1 1) ϕ-scan was found to be 7° FWHM. The FWHM for the out-of-plane texture as determined by a ω-scan was found to be 6.1° and 8.8° for rocking in and about the rolling direction. The GBMD obtained using EBKD from this substrate indicates that the distribution of grain boundaries is centered at 5.5° with a FWHM of ~6°. Clearly, a predominance of low-angle grain boundaries is present. Upon annealing at 1400 °C, the texture sharpened considerably with

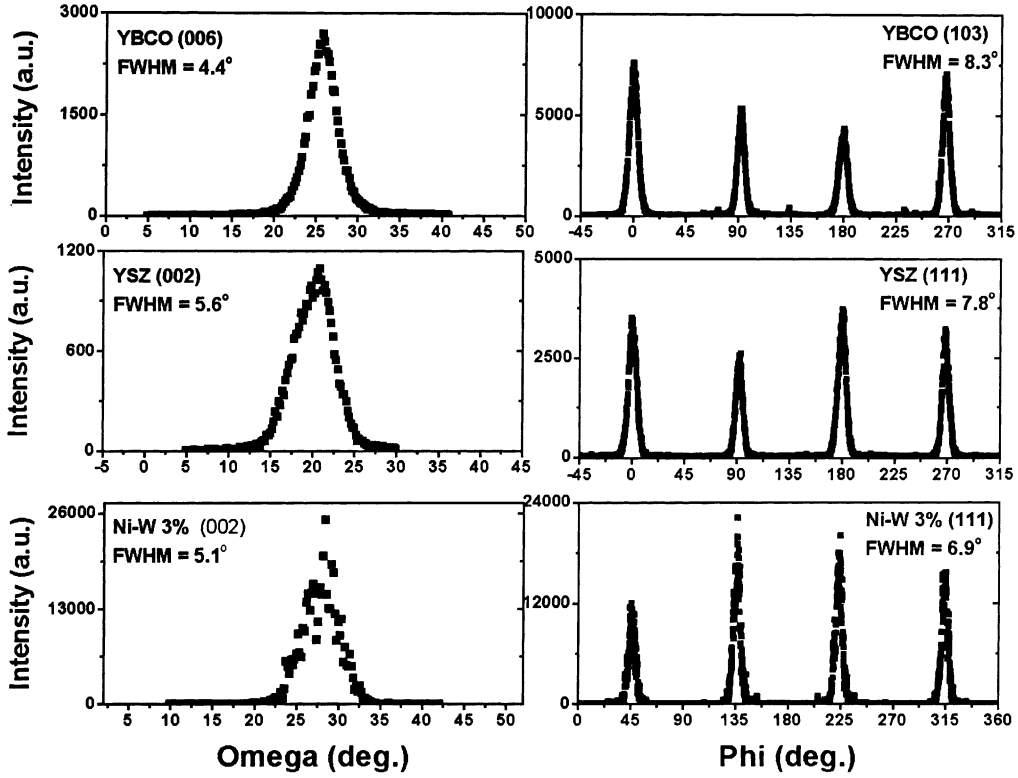

Fig. 9. Out-of-plane and in-plane textures for a 1 cm wide YBCO/CeO_2/YSZ/Y_2O_3/Ni–3at.%W–1.7at.%Fe sample. X-ray Θ-scans taken by rocking *in* the rolling direction show that the FWHM for the Ni, YSZ and YBCO layers was 5.1°, 5.6° and 4.4° respectively. X-ray ϕ-scans for the Ni, YSZ and YBCO layers show a FWHM of 6.9°, 7.8° and 8.3° respectively.

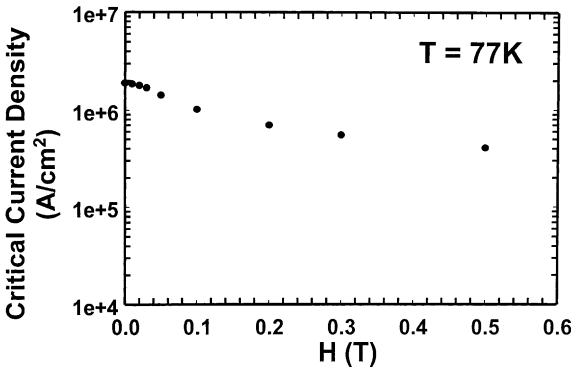

Fig. 10. J_c versus applied magnetic field for the 1 cm wide YBCO/CeO_2/YSZ/Y_2O_3/Ni–3at.%W–1.7at.%Fe sample at 77 K.

the FWHM of the in-plane texture decreasing to 5.8°. The out-of-plane texture also sharpened to FWHM of 4.3° and 7.4° respectively. It is expected that at this annealing condition, the GBMD is skewed more towards lower misorientation angles.

The YS of the Ni–3at.%W–1.7at.%Fe substrate was determined to be 143 and 154 MPa at 0.02% and 0.2% strain respectively. Similar tests for 99.99% Ni (metals basis) show a YS of 40 and 58 MPa at 0.02% and 0.2% strain respectively with the Ni substrates also made using powder metallurgy and having a similar grain size, thickness and annealing condition. Hence, the Ni substrate with minor alloying additions of W and Fe is significantly stronger than the 99.99%Ni substrate.

The Ni–3at.%W–1.7at.%Fe substrate was ferromagnetic at room temperature. Examination of magnetic properties at cryogenic temperatures show that the magnetization, M, varies very little for temperatures below ~150 K. The field dependence of M at 100 K, for fields up to 65 kOe, revealed a "square" response characteristic of a soft ferromagnet. The saturation magnetization was found to be 40 G cm^3/g, significantly below that of pure Ni (57.5 G cm^3/g at $T = 0$).

Epitaxial seed oxide layers of CeO_2, Y_2O_3 and RE_2O_3 could be deposited on the Ni–3at.%W–1.7at.%Fe substrate without any additional surface modification steps to obtain a cube-on-cube epitaxy. This is technologically quite significant since any additional steps make the process more complicated and expensive for scaling up to long lengths. RHEED patterns obtained from the surface of the Ni–3at.%W–1.7at.%Fe substrate indicate the presence of a c(2 × 2) 2-D superstructure, similar to that obtained on the surface of cube textured 99.99% Ni substrate. It is believed that presence of this superstructure allows deposition of oxide layers directly on the Ni–3at.%W–1.7at.%Fe substrate without any intermediate metal buffer layers.

High critical current densities, up to 1.9 MA/cm^2 at 77 K, self-field were demonstrated on this substrate using a multilayer configuration YBCO/CeO_2/YSZ/Y_2O_3/Ni–3at.%W–1.7at.%Fe. This translates to a I_c of 59 A/cm width. J_c at 0.5 T reduced by only 21% indicating strongly-linked grain boundaries in the YBCO film on this substrate.

Acknowledgements

Research sponsored by the US Department of Energy under contract no. DE-AC05-00OR22725 with the Oak Ridge National Laboratory, managed by UT-Battelle, LLC.

References

[1] X.D. Wu, S.R. Foltyn, P.N. Arendt, W.R. Blumenthal, I.H. Campbell, J.D. Cotton, J.Y. Coulter, W.L. Hults, M.P. Maley, H.F. Safar, J.L. Smith, Appl. Phys. Lett. 67 (1995) 2397.
[2] K. Hasegawa, N. Yoshida, K. Fujino, H. Mukai, K. Hayashi, K. Sato, Y. Sato, S. Honjo, T. Ohkuma, H. Ishii, T. Hara, in: S. Nakajima, M. Murakami (Eds.), Advances in Superconductivity IX, Proceedings of the 9th International Symposium on Superconductivity (ISS'96), Sapporo, Japan, 1996, p. 745.
[3] A. Goyal, D.P. Norton, J.D. Budai, M. Paranthaman, E.D. Specht, D.M. Kroeger, D.K. Christen, Q. He, B. Saffian, F.A. List, D.F. Lee, P.M. Martin, C.E. Klabunde, E. Hatfield, V.K. Sikka, Appl. Phys. Lett. 69 (1996) 1795.
[4] A. Goyal et al., US Patents: 5, 739, 086; 5, 741, 377; 5, 846, 912; 5, 898, 020; 5, 964, 966; 5, 958, 599; 5, 968, 877.
[5] A. Goyal, D.P. Norton, et al., Special 10th anniversary on high temperature superconductors, J. Mater. Res. 12 (1997) 2924–2940.
[6] J.E. Mathis, A. Goyal, D.F. Lee, F.A. List, M. Paranthaman, D.K. Christen, E.D. Specht, D.M. Kroeger, P.M. Martin, Jpn. J. Appl. Phys. 37 (1998) L1379.
[7] A. Goyal et al., US Patent Nos. 5, 964, 966 and 6, 106, 615.
[8] A. Goyal, unpublished results.

[9] M. Paranthaman, D.F. Lee, A. Goyal, E.D. Specht, P.M. Martin, X. Cui, J.E. Mathis, R. Feenstra, D.K. Christen, D.M. Kroeger, Supercond. Sci. Technol. 12 (1999) 319.
[10] J.S. Morrell, Z.B. Xue, E.D. Specht, A. Goyal, P.M. Martin, D.F. Lee, R. Feenstra, D.T. Verebelyi, D.K. Christen, T.G. Chirayil, M. Paranthaman, C.E. Vallet, D.B. Beach, J. Mater. Res. 15 (2000) 621–628.
[11] F.A. List, A. Goyal, M. Paranthaman, D.P. Norton, E.D. Specht, D.F. Lee, D.M. Kroeger, Physica C 302 (1998) 87–92.
[12] D.F. Lee, M. Paranthaman, J.E. Mathis, A. Goyal, D.M. Kroeger, E.D. Specht, R.K. Williams, F.A. List, P.M. Martin, C. Park, D. Norton, D.K. Christen, Jpn. J. Appl. Phys. 38 (1998) L178.
[13] R. Feenstra, T.B. Lindemer, J.D. Budai, M.D. Galloway, J. Appl. Phys. 69 (1991) 6569.
[14] S.W. Lu, F.A. List, D.F. Lee, X. Cui, M. Paranthaman, B.W. Kang, D.M. Kroeger, A. Goyal, P.M. Martin, R.E. Ericson, Supercond. Sci. Technol. 14 (4) (2001) 218–223.
[15] A. Goyal, S.X. Ren, E.D. Specht, D.M. Kroeger, R. Feenstra, D. Norton, M. Paranthaman, D.F. Lee, D.K. Christen, Micron 30 (1999) 463.
[16] R.P. Bozorth, in: Ferromagnetism, IEEE Press, Piscataway, NJ, 1978, pp. 307–308.
[17] H.P.J. Wijn (Ed.), Magnetic Properties of Metals, Landolt–Bornstein New Series III/19a, Springer, Heidelberg, 1986, p. 563.
[18] C. Cantoni, D.K. Christen, R. Feenstra, A. Goyal, G.W. Ownby, D.M. Zehner, D.P. Norton, Appl. Phys. Lett. 79 (19) (2001) 3077–3079.